

Diversion of plasma due to high pressure in the inner magnetosphere during steady magnetospheric convection

J. Kissinger,^{1,2} R. L. McPherron,^{1,2} T.-S. Hsu,^{1,2} and V. Angelopoulos^{1,2}

Received 2 February 2012; revised 18 March 2012; accepted 19 March 2012; published 3 May 2012.

[1] Steady magnetospheric convection (SMC) events in the Earth's magnetosphere are thought to result from balancing the rate of opening flux through solar wind-magnetosphere reconnection at the dayside magnetopause to the rate of closing flux through reconnection in the magnetotail. For this to occur, reconnected flux in the tail must return to the dayside to balance the dayside reconnection rate. Using Geotail and THEMIS data over a span of 14 years, we examine the average plasma conditions and fast Earthward flows during SMC intervals and compare them to other types of geomagnetic activity, such as quiet intervals, isolated substorm phases, and the two hours before an SMC (Pre-SMC intervals). We show that the average total pressure in the inner magnetosphere is higher during SMC events than for other types of activity. This higher pressure region extends to larger radial distances, and causes fast Earthward flows to divert toward the dawn or dusk flanks and continue to the dayside. This pattern is contrasted to substorms, during which flows are directed toward the inner magnetosphere and flux remains there in the "pile-up region." We suggest that the SMC pattern of flow deflection carries enough flux from the tail to the dayside to allow for balanced reconnection. Finally, the Pre-SMC intervals have plasma conditions that are similar to, but slightly weaker than, SMC events. Since most SMCs begin with a substorm, this indicates that preconditioning of the magnetosphere by prior geomagnetic activity is important in setting up the magnetotail for an SMC state.

Citation: Kissinger, J., R. L. McPherron, T.-S. Hsu, and V. Angelopoulos (2012), Diversion of plasma due to high pressure in the inner magnetosphere during steady magnetospheric convection, *J. Geophys. Res.*, *117*, A05206, doi:10.1029/2012JA017579.

1. Introduction

[2] When the solar wind Interplanetary Magnetic Field (IMF) has a negative B_z component, i.e., is southward, it can reconnect with the Earth's northward-pointing dipole magnetic field. Reconnection drives geomagnetic activity by opening dayside magnetic flux and transporting it to the nightside. Open field lines are pulled back by the solar wind to form the magnetotail lobes. The north and south tail lobes reconnect on the nightside and create the closed field lines of the plasma sheet. The pressure gradient between dayside and nightside causes Sunward flow, driving convection back toward the Earth, in a process known as the Dungey cycle [Dungey, 1961]. The Earth's magnetosphere responds to solar wind driving in various ways. One of the most well-studied modes of response is the substorm, a loading-unloading

process in which energy builds up in the magnetotail during a growth phase [McPherron, 1970], is suddenly released in an expansion phase, and declines back to quiet values in the recovery phase [Russell and McPherron, 1973]. Other times, the magnetosphere can respond with a quasi-steady response known as steady magnetospheric convection (SMC). These events are characterized by enhanced, stable convection, persisting longer than a typical recovery phase, with no substorm expansions [Pytte *et al.*, 1978; Sergeev *et al.*, 1996].

[3] Why the magnetosphere sometimes responds with a substorm and sometimes with an SMC event is still unknown. One possible factor that could contribute to the response is preconditioning of the magnetosphere. O'Brien *et al.* [2002] identified two cases where the solar wind velocity and IMF B_z were similar, but one resulted in an isolated substorm and the other in an SMC. They pointed out that before the SMC occurred, the magnetosphere was already undergoing enhanced activity, while before the isolated substorm, the magnetosphere was quiet. In fact, about 80% of SMCs are associated with an obvious substorm expansion onset just before the start of the SMC [McPherron *et al.*, 2005]. In most statistical SMC studies, events without a preceding substorm onset are the exception [DeJong *et al.*, 2009; Dmitrieva *et al.*, 2004]. This preceding substorm may change the conditions in the magnetosphere to allow an SMC to occur.

¹Department of Earth and Space Sciences, University of California, Los Angeles, California, USA.

²Institute of Geophysics and Planetary Physics, University of California, Los Angeles, California, USA.

Corresponding Author: J. Kissinger, Department of Earth and Space Sciences, University of California, Los Angeles, CA 90095, USA. (jkissinger@ucla.edu)

Copyright 2012 by the American Geophysical Union. 0148-0227/12/2012JA017579

[4] SMC events are thought to occur from balanced reconnection rates between the dayside and nightside reconnection x-lines. *Dmitrieva et al.* [2004] showed this balance by comparing average dayside merging electric field and average plasma sheet electric field during SMCs and substorms. They found that the two flux transport rates were equal during SMC events; by comparison, the plasma sheet convection was reduced during substorm growth phases and twice as large during substorm expansions, compared to the dayside flux transport rate. In studying flux transport rates, statistical averages of multiple events are necessary because plasma sheet convection consists of both “quiet” convection and fast short-duration flows [*Baumjohann et al.*, 1989, 1990]. These variations were identified during substorms as bursty bulk flows (BBFs), a series of fast-moving plasma bursts a few Earth radii (R_E) wide that carry closed magnetic flux from the nightside tail reconnection region [*Angelopoulos et al.*, 1992, 1994]. Earthward BBFs concurrent with positive B_z are a signature that enhanced reconnection has occurred tailward of the flow. During substorms, BBFs are decelerated in the inner magnetosphere, where the dipole field strength increases. As more BBFs are slowed and stopped, a “pile-up region” of magnetic flux is formed and grows radially outward [*Baumjohann et al.*, 1999]. The occurrence of BBFs increases as the auroral electrojet index (AE) increases [*Angelopoulos et al.*, 1994], and BBFs can account for a majority of observed Earthward flux transport [*Angelopoulos et al.*, 1994; *Schödel et al.*, 2001]. Fast flows are even observed when the magnetosphere is quiet [*Angelopoulos et al.*, 1993].

[5] Although we refer to “steady convection” for SMCs, in reality these events also consist of fast plasma flow bursts that can carry 11–84% of the mass flux in a given event [*Sergeev et al.*, 1990, 1996]. *Tanskanen et al.* [2005] also found BBFs during periods of relatively steady magnetotail total pressure (called continuous magnetospheric dissipation (CMD) events). Compared to an unloading mode (substorm expansion), BBFs during CMD events are not as fast but occur more often. Recent models also indicate strong flows during SMC events, with Earthward flowing plasma diverted to the dawn and dusk flanks, leaving the inner magnetosphere undisturbed [*Goodrich et al.*, 2007]. Using a set of nine events, *Yang et al.* [2010] indicated that during SMC-associated fast flows, the entropy parameter remains nearly constant, indicating mid-tail reconnection.

[6] During substorms, the flux pile-up region keeps a portion of tail-reconnected flux from returning to the dayside reconnection region. In an SMC, the tail-reconnected flux should return to the dayside in order to continue balancing the dayside reconnection rate for hours at a time, but how the tail accomplishes this flux return remains unknown. To investigate this question, we perform a detailed statistical analysis of fast flows and plasma conditions in the magnetotail during SMC events. The results are compared to flows and plasma during quiet intervals, pre-SMC intervals, and substorm phases.

2. Data and Event Selection

[7] All modes of response were identified with auroral index data, AL (auroral lower) and AU (auroral upper), from the World Data Center for Geomagnetism, Kyoto AE index service. SMC events were visually selected between 1997

and 2010 according to the criteria of *Kissinger et al.* [2011]. Briefly summarized, the criteria are 1) $AL < -75$ nT; 2) $AU > 50$ nT; 3) AL steadiness (or coefficient of variance, the standard deviation divided by the mean) $< 20\%$; 4) 10 nT/min $> dAL/dt > -7.4$ nT/min (where dAL/dt is a 15 min sliding derivative operator that represents the rate of change in the AL index) and 5) event duration > 90 min. We found 2853 intervals satisfying these criteria. To investigate the role of magnetospheric preconditioning in SMCs, we also look at the two hour interval before the start of an SMC, hereafter dubbed Pre-SMC.

[8] Substorm onsets were selected visually from auroral indices, characterized by a sharp drop in the AL index (T.-S. Hsu and R. L. McPherron, A statistical analysis of substorm associated tail activity, submitted to *Advances in Space Research*, 2012). The subset of onsets we examine here occurred during 1997–2010. To be certain that the substorm was distinct from the SMC, it was required that the onset occurred more than 75 min before the start of an SMC; i.e., not a substorm associated with SMC. Further, we attempted to select “isolated” substorms by requiring that for a given onset, there could not be another onset within ± 2.5 h. This resulted in 8600 substorm onsets. Using the time of the onset, we identified the three phases of a substorm: growth, expansion, and recovery. We began the growth phase intervals -30 min before the onset and set the end of the growth intervals as the onset. Expansion phase intervals were chosen by setting the onset as the start of the event, and setting the end of the interval $+30$ min after the onset [*McPherron*, 1970]. Finally, recovery phase intervals were selected from onset $+45$ min to onset $+120$ min [*Baker et al.*, 1994; *Baumjohann et al.*, 1991]. Although this is a crude measure of substorm phases, the authors are not aware of a current, large list of substorm phases.

[9] Quiet intervals were selected automatically with auroral indices by requiring that $AL > -75$ nT and $AU < 50$ nT for at least 90 min. The quiet events spanned the interval 1997–2010. The identified events resulted in far more data than necessary, so every fifth event was selected. The final list included 1422 quiet events.

[10] We used data sets from two missions for this study: the Geotail satellite and all five THEMIS probes. Geotail data was supplied by the CDAWeb website. Magnetic field components came from the Magnetic Field Instrument (MGF), and plasma moments came from the Low-Energy Particles Instrument (LEP), which measures an energy range of 60 eV to 40 keV for ions. The temporal coverage of available Geotail data is from 1997 to 2006. Geotail provides two types of data: Editor-A, which is transmitted in real-time to the Usuda Deep Space Center in Japan, and Editor-B, which is recorded continuously onboard the satellite and then downloaded daily to the NASA JPL Deep Space Network [*Nishida*, 1994]. We used Editor-A when it was available, since it is considered more reliable, and Editor-B at all other times [*Mukai et al.*, 1994]. The magnetic field components were downloaded in Geocentric Solar Magnetospheric (GSM) coordinates at 3-s cadence, and a B_z offset correction was applied based on values from the Geotail website. This was interpolated to 12-s cadence to match the plasma data. The THEMIS magnetic field data consists of Level 2 fluxgate magnetometer spin fit (FGS) components in GSM coordinates. Plasma moments from the

lower energy electrostatic analyzer (ESA, ranging from a few eV to 30 keV for electrons and 25 keV for ions) and higher energy solid state telescope (SST, ranging from 25 keV to 6 MeV) instruments were computed on the ground and then added together to obtain combined moments. All parameters were interpolated to the same 12-s cadence as Geotail plasma data. THEMIS data was used for events during 2007–2010.

[11] By combining these two data sets, we were able to obtain results from over an entire solar cycle (Geotail from 1997 to 2006, THEMIS from 2007 to 2010), as well as greater coverage of radial distances. THEMIS data was limited to an inner radial distance (ρ) boundary of $\rho \geq 5 R_E$. The majority of THEMIS data points occur within 12 R_E , the apogee of three of the spacecraft, but data farther out was also obtained from the B (apogee of 30 R_E) and C (apogee of 20 R_E) spacecraft. We restricted Geotail data to a radial distance of $\rho \geq 12 R_E$, since we did not have the high energy particle data that could affect the moments inside this region. Beyond this distance, the energetic particle contribution is small. Thus we obtain greater temporal and spatial coverage than could be obtained by either mission alone.

[12] In sections 3 and 4, we present results from ion flows and moments. One exception is the total pressure, which was calculated differently between Geotail and THEMIS. For Geotail, only ion LEP data was available, and thus the electron pressure component is not included in the total pressure. Geotail dominates outside of 13 R_E , where electron pressure is very small, yet THEMIS dominates inside of 13 R_E , where electron pressure starts becoming considerable. Therefore both the electrons and ions were used to calculate the pressure for the THEMIS data set. This means that we might underestimate the average total pressure in the region where Geotail dominates the coverage, though the relative differences between the modes of response in this region should be the same. In order to confirm that we can legitimately combine the two data sets, we compared plasma moments between Geotail and THEMIS from the region of comparable overlap, $\rho = 13\text{--}16 R_E$. Histograms of the moments were in agreement between the two missions; in particular, the total pressure histograms were very similar. This confirms that the electron pressure contribution is small beyond 13 R_E and validates our combination of the two data sets.

3. Earthward Fast Flow Bursts

[13] We set out to identify fast flow patterns in the magnetotail, and thus limited our data set to times when a spacecraft was within $X_{GSM} \leq 0 R_E$ and $|Y_{GSM}| \leq 20 R_E$. Furthermore, we attempted to remove data within the magnetosheath by excluding points when the following was true: $|Y_{GSM}| > 11 R_E$, ion temperature (T_i) < 0.5 keV, and ion density (n_i) $> 1 \text{ cm}^{-3}$. Data was restricted to the plasma sheet by requiring that beta (β), the ratio of the plasma pressure ($P_{th} = nkT$) to the magnetic pressure ($P_{mag} = \frac{B_z^2}{2\mu_0}$), be greater than 0.5. Finally, the time-averaged velocity vector was separated into parallel and perpendicular vectors based on the magnetic field. Hereafter when we refer to the velocity, we are referring to the perpendicular velocity vector (\mathbf{V}_{perp}) unless otherwise stated.

[14] Fast Earthward flows were defined when $V_{x-y} \geq 200$ km/s, where V_{x-y} is the total speed in the GSM x-y plane, and $V_x > 0$ km/s. The start of the flow was selected when the equatorial speed exceeded 200 km/s, and the end selected when the speed fell below 200 km/s. An example of fast flows during SMC observed by Geotail is presented in Figure 1. The spacecraft passed in and out of the plasma sheet (β , fifth panel) throughout the interval, and whenever it was in the plasma sheet, it saw fast Earthward flows (\mathbf{V}_{perp} , third panel). Although the AL index was weak and steady (first panel), there was significant transient activity in the tail. Geotail was located at $|X| \sim 28 R_E$, indicating nightside reconnection occurred tailward of this point. The fast plasma flows are responsible for a significant transport of magnetic flux (fourth panel).

[15] Table 1 compiles the number of events and the number of Earthward fast flows observed during quiet, Pre-SMC, SMC, and substorm phase intervals. SMCs have the highest occurrence rate of Earthward fast flows (3.8%), followed by Pre-SMC (2.5%), substorm recovery (1.8%), substorm expansion (1.5%), and substorm growth (1.1%). As expected, quiet periods show the lowest occurrence of fast flows (0.3%), although they are still observed [Angelopoulos *et al.*, 1993]. The occurrence of SMC fast flows correlates to Tanskanen *et al.* [2005], who found that more fast flows occurred during intervals of relatively steady tail total pressure (termed continuous magnetospheric dissipation) compared to unloading intervals. Previous study of BBFs has shown that in some cases, they can comprise more than 80% of Earthward magnetic flux transport [Angelopoulos *et al.*, 1994]. In the last column of Table 1, we show the overall average of Earthward flux transport accomplished by Earthward fast flows for each type of activity. Earthward magnetic flux transport rate is defined as the equatorial speed V_{x-y} times B_z when the velocity has an Earthward component ($V_x > 0$ km/s). The amount of transported flux is the time integral of this rate. To obtain the percentage of flux transport, we integrate the flux observed by the spacecraft during Earthward fast flows and divide it by the total Earthward flux transport observed throughout the event. The largest percentage of fast flow Earthward magnetic flux transport is during Pre-SMC and SMC cases, with $\sim 15\%$ and $\sim 20\%$ of the total Earthward flux transport accomplished by fast flows, respectively. These values are consistent with prior SMC case studies that found individual event fast flow occurrence rates of 2–27% and fast flow flux transport levels of 11–84% [Sergeev *et al.*, 1996]. This is also comparable to the event in Figure 1, in which fast Earthward flows are observed during 23% of this event, carrying 68% of the magnetic flux during the SMC interval.

[16] The probability of observing fast Earthward flows is further illustrated in Figures 2 and 3. Figure 2 plots the probability of observing a fast Earthward flow versus radial distance during each of the six types of activity: quiet (purple), Pre-SMC (orange), SMC (black), substorm growth (green), substorm expansion (blue), and substorm recovery (red). All probabilities have been normalized to the time spent in each 0.2 R_E bin by the satellites. SMC events show the highest probability of fast flows in the mid-tail (distance $> 21 R_E$), followed next by substorm recovery. The probability of observing fast Earthward flows during SMCs increases approximately linearly as radial distance increases,

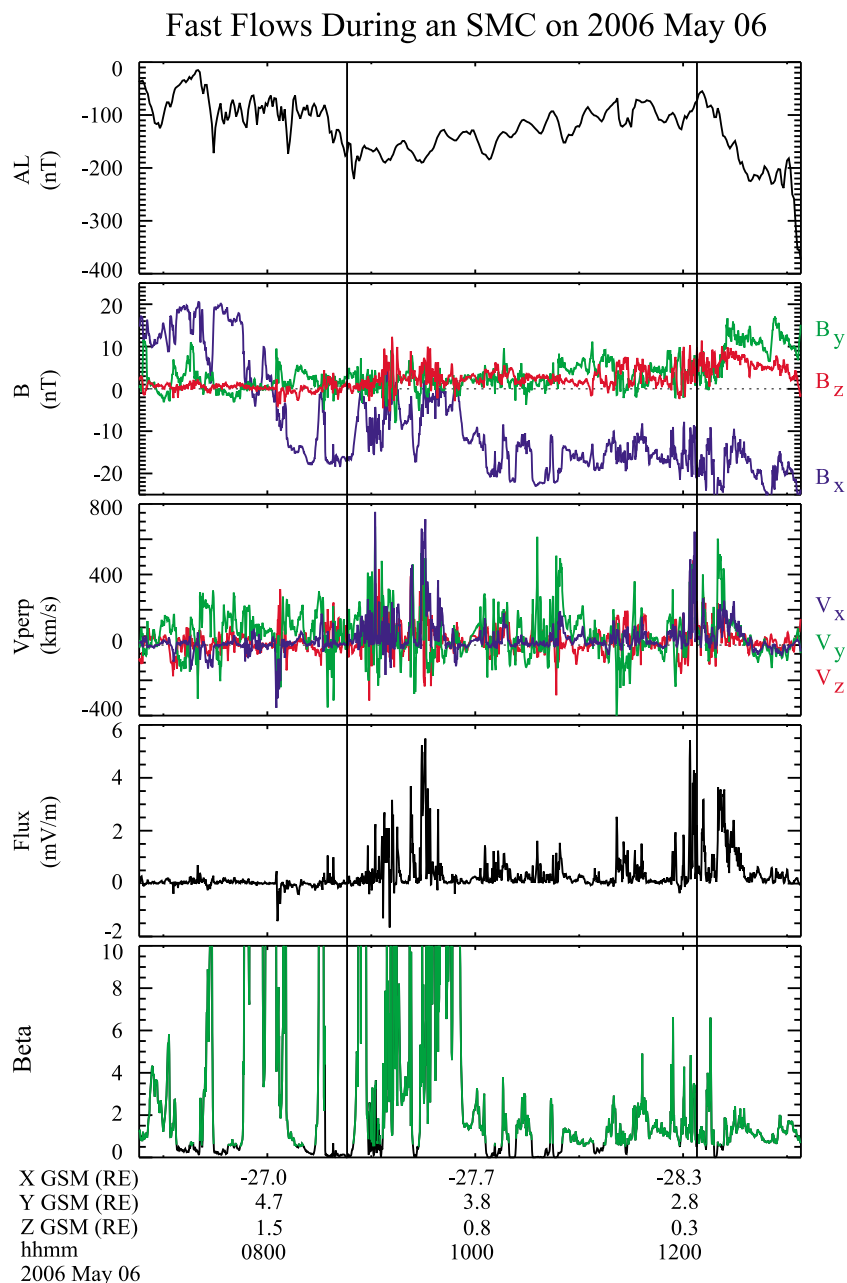


Figure 1. An example of fast Earthward flow bursts that occurred during an SMC event on 06 May 2006. The SMC began at 0846 UT (vertical black line) and ended at 1208 UT. The panels show AL index, magnetic field components in GSM coordinates from Geotail, perpendicular velocity components from Geotail, flux transport ($\text{flux} = V_{x-y} * B_z$), and beta (ρ_{th} / ρ_{mag}). Beta is marked in green when the spacecraft was in the plasma sheet ($\beta > 0.5$).

Table 1. Earthward Fast Flows by Mode of Response

Response	Number of Events	Data Hours	Number of Earthward Flows	Occurrence Rate (%)	Earthward Transport (%)
Quiet	1422	2972	1045	0.3	4.2
Pre-SMC	2853	1034	2692	2.5	15.4
SMC	2853	1505	5653	3.8	20.1
Substorm growth	8600	1147	1337	1.1	9.0
Substorm expansion	8600	1113	1859	1.5	12.2
Substorm recovery	8600	2986	5349	1.8	13.4

Probability of Earthward Fast Flows vs. Radial Distance

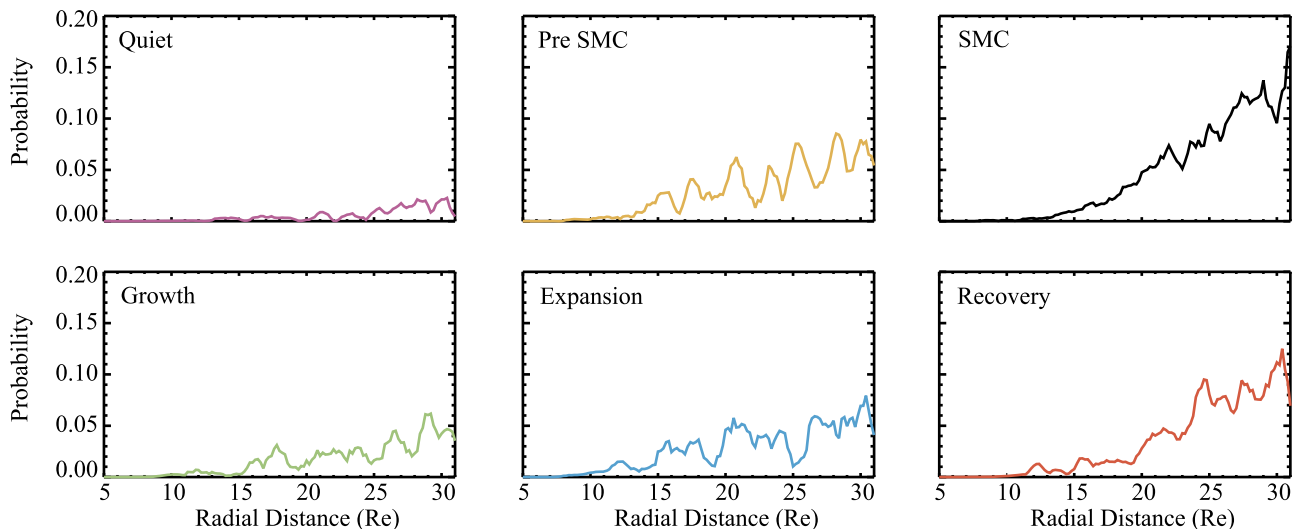


Figure 2. The probability of observing fast ($V_{x-y} > 200$ km/s) Earthward flows in the magnetotail by radial distance. Occurrence of flows was normalized by the amount of time spent by spacecraft in each bin. Each plot represents a different level of geomagnetic activity: (top left) quiet (purple), (top middle) pre-SMC (orange), (top right) SMC (black), (bottom left) substorm growth (green), (bottom middle) substorm expansion (blue), and (bottom right) substorm recovery (red).

with the highest probability occurring at 31 R_E , the apogee of the Geotail and THEMIS B spacecraft. This indicates that during SMCs, the average location of the tail x-line is beyond 31 R_E . The probability during substorm recovery likewise increases in a mostly linear fashion as radial distance increases. In contrast, Pre-SMC and substorm expansion intervals show more variation, with peaks and troughs in probability. In the inner magnetosphere (within 15 R_E), the probability of seeing a fast Earthward flow during SMC

becomes smaller than the probability during substorm expansion or recovery. The quiet and growth phases have lower overall probabilities of seeing fast flows.

[17] Figure 3 is similar to Figure 2, but displays fast Earthward flow probability versus local time (LT) in 0.5 h bins. For all types of activity, the probability of observing fast Earthward flows has approximately the same distribution shape versus local time, with the highest probabilities near midnight and the lowest on the dawn and dusk flanks,

Probability of Earthward Fast Flows vs. Local Time

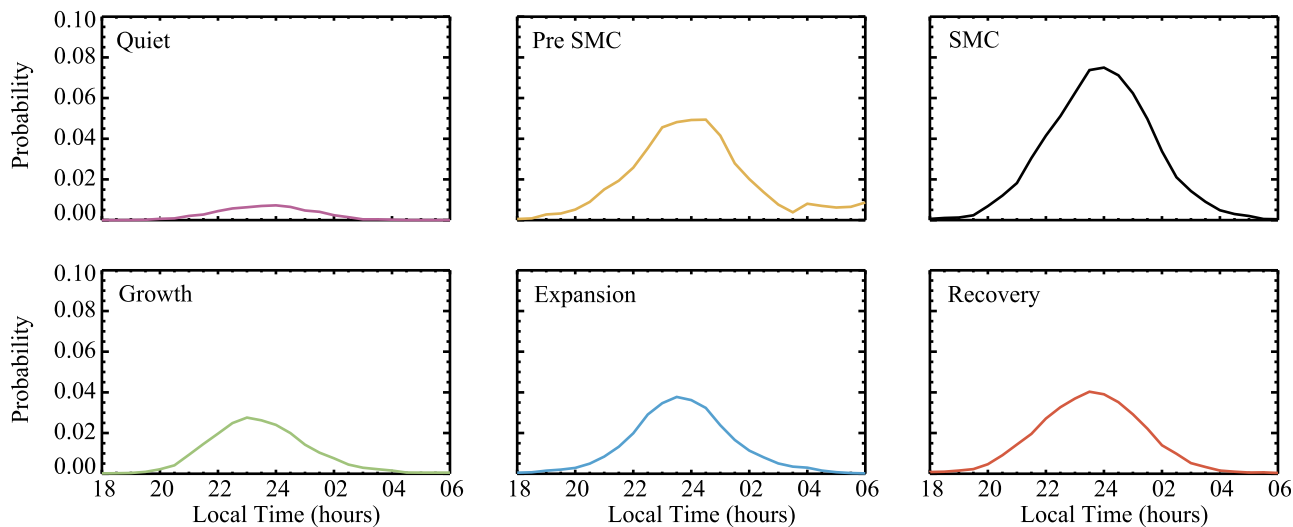


Figure 3. The probability of observing fast ($V_{x-y} > 200$ km/s) Earthward flows in the magnetotail by local time (same layout as Figure 2).

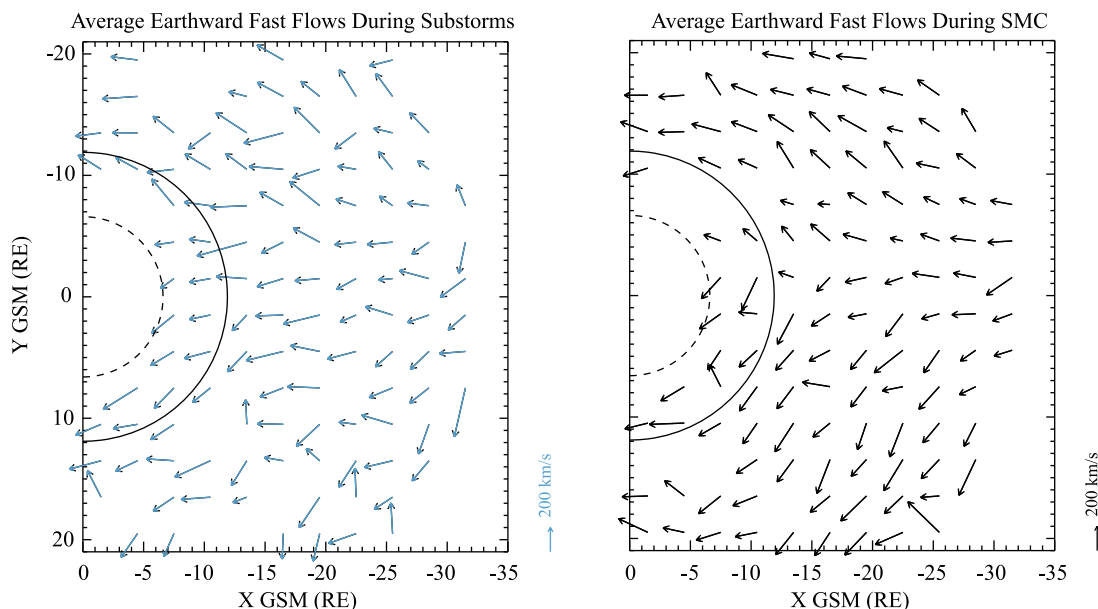


Figure 4. Average fast Earthward flow vectors during (left) substorm expansions and (right) SMCs. Flows were averaged into $3 \times 3 R_E$ bins and are plotted in the GSM x-y plane. The dashed semicircle represents geosynchronous orbit ($6.6 R_E$) and the solid semicircle represents the apogee of the THEMIS D and E spacecraft ($11.9 R_E$). Flows are scaled to 200 km/s (right arrow key).

in agreement with previous statistical results [Angelopoulos *et al.*, 1994]. SMC and Pre-SMC flow probabilities are peaked at midnight (2400 LT), while the substorm growth distribution is centered at 2300 LT and substorm expansion and recovery distributions are centered at 2330 LT. McPherron *et al.* [2011] found a similar result during substorms with inner magnetosphere fast flows peaking at 2300 LT.

[18] To create patterns of fast flows for each type of activity, fast Earthward flows were averaged in $3 \times 3 R_E$ bins, and an equatorial map created of the average binned vectors in the GSM x-y plane. Figure 4 shows the average Earthward fast flow vectors for substorm expansions (left) and SMC events (right). We only compare two of these panels to avoid visual confusion, and selected substorm expansion intervals to highlight the most significant differences from the SMC pattern. The dashed semi-circle line represents geosynchronous orbit ($6.6 R_E$), and the solid semi-circle line represents the apogee of THEMIS D and E, two of the inner probes. The arrow key on the right is 200 km/s. This figure is a visual average over all events, and does not imply that for any single event, that fast flows are seen throughout the entire tail. Lack of vectors indicates that no fast flows were observed in that bin.

[19] Fast Earthward flows during SMC events show a very clear pattern of deflection toward either the duskward or dawnward flank. This deflection is small along the midnight line, but is seen on either side of midnight and increases with $|Y|$. Flow deflection also appears to increase as radial distance decreases. This statistical pattern concurs with two SMC events in Sergeev and Lennartsson [1988], who showed strong flankward components on both the duskward and dawnward side of the tail, following modeled contours of constant flux tube volume. This pattern is much more symmetric around midnight compared to previous studies of

average flow patterns, such as Angelopoulos *et al.* [1993] and Hori *et al.* [2000]. These studies found that the average flow pattern displayed a dawn-dusk asymmetry, with smaller and sunward-directed flows in the dawn flank and larger, duskward-directed flows in the dusk flank. However, fast flows were removed in Angelopoulos *et al.* [1993] and averaged in Hori *et al.* [2000]. The larger duskward component in these slower flow patterns was due to the diamagnetic drift of ions due to the inward pressure gradient, which has a magnitude on the order of 25 km/s [Angelopoulos *et al.*, 1993]. Since this duskward drift is much smaller than our 200 km/s fast flow cutoff, it has a negligible effect on our flow patterns.

[20] Fewer fast flows are observed in the inner magnetosphere (within the solid curved line at $11.9 R_E$) for SMCs compared to substorms. This agrees with the radial flow probabilities from Figure 2, as well as results from McPherron *et al.* [2011]. The lower probability of observing a fast flow during SMC events is shown numerically in Table 2. For each type of activity we show the total number of Earthward fast flows that occur within $15 R_E$, their occurrence rate, and the percentage of earthward magnetic flux transport they contribute. Fewer fast flows are observed during SMC than for Pre-SMC or substorm intervals, with

Table 2. Earthward Fast Flows Within $15 R_E$

Response	Number of Earthward Flows	Occurrence Rate (%)	Earthward Transport (%)
Quiet	151	0.06	1.6
Pre-SMC	230	0.41	4.5
SMC	156	0.18	1.6
Substorm growth	242	0.22	6.8
Substorm expansion	521	0.50	3.8
Substorm recovery	415	0.20	2.8

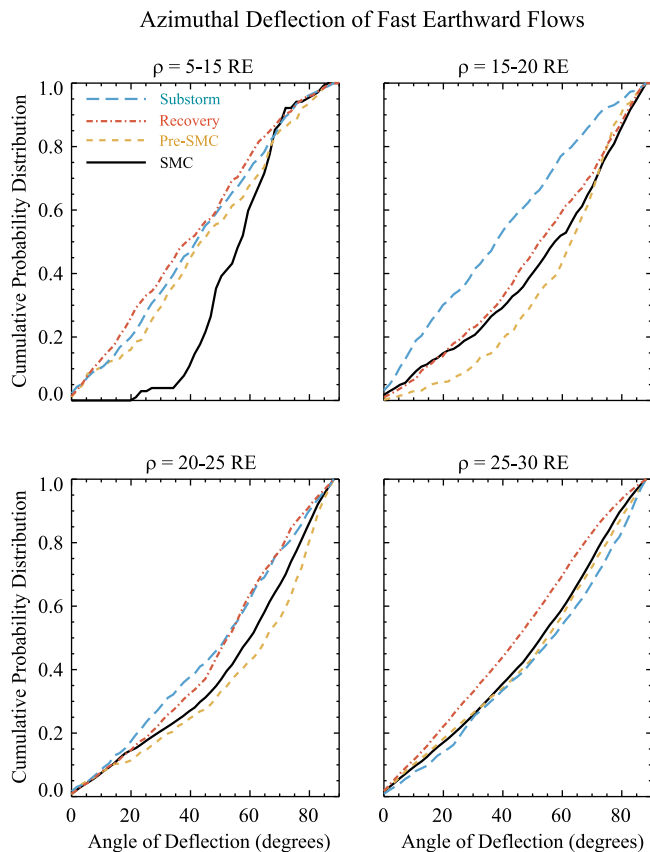


Figure 5. Cumulative probability distributions of the absolute azimuthal deflection of fast Earthward flows. The deflection is measured with respect to the X-GSM axis, such that 0° is along the x axis (Earthward) and 90° is along the Y-GSM axis (dawnward or duskward). Four types of activity are shown: substorm expansion (blue long dashed lines), substorm recovery (red dash-dotted lines), Pre-SMC (orange short dashed lines) and SMC (black solid lines). Only fast flows within 2300–0100 LT are included. The plots represent different radial distances: (top left) 5–15 R_E , (top right) 15–20 R_E , (bottom left) 20–25 R_E , and (bottom right) 25–30 R_E .

the most earthward fast flows observed during substorm expansion phases. In contrast to the SMC case, during substorms fast Earthward flows show a pattern of more directly Earthward flow, especially in the midnight region of the tail ($|Y| < 7 R_E$). There is some deflection toward the flanks away from the midnight region, although the pattern is somewhat unclear.

[21] To quantitatively illustrate this visual result, we examine the deflection angle of the fast flows. For each flow burst near midnight (within 2300–0100 LT), we measured the absolute angle between the X-GSM axis and the flow (so that an angle of 0° would be directly along the X-GSM axis or Earthward, while 90° would be along the Y-GSM axis or flankward). Figure 5 plots the cumulative probability distributions of deflection angle for flows during SMC (black), Pre-SMC (orange), substorm expansion (blue) and substorm recovery (red) within radial distances of (top left) 5–15 R_E , (top right) 15–20 R_E , (bottom left) 20–25 R_E , and (bottom right) 25–30 R_E . Starting with the outer-most radial

distances (bottom plots), in the mid-tail, the distributions of deflection angle are similar. Flows are equally Earthward or flankward for all four types of activity. As we move radially inward to within 20 R_E (upper right), substorm expansion fast flows are slightly less deflected, SMC and substorm recovery fast flows are more deflected, and Pre-SMC fast flows experience the most deflection. Within 15 R_E (upper left), the situation changes dramatically. Substorm expansion and recovery fast flows have the least deflection, Pre-SMC fast flows have become significantly more Earthward-directed to match the substorm distributions, and SMC fast flows experience very significant deflection toward the flanks. In fact, there is a 0% probability that SMC fast flows are within 20° of the X-GSM line (Earthward), and only 5% probability that they are within 35° .

[22] In the next section, we will explore further what causes the diversion of fast flows during SMC events.

4. Plasma Conditions in the Magnetotail

[23] In this section, we examine the average behavior of plasma density, temperature, pressure, and Earthward flux transportation rates in the magnetotail during the six types of activity. All plasma sheet ($\beta > 0.5$) data from the Geotail and THEMIS satellites were compiled to create spatial event ensembles. We will show that the average conditions in the magnetotail are very different depending on the mode of magnetospheric response.

[24] Figure 6 shows contours of average ion density (cm^{-3}) in the GSM equatorial plane for quiet, Pre-SMC, SMC, substorm growth, substorm expansion, and substorm recovery. All plots are to the same color scale. The green circle in the middle of each plot represents Earth, and the larger dashed circle is geosynchronous orbit ($6.6 R_E$). In each case, the density is highest in the inner magnetosphere and lowest in the tail. The SMC and Pre-SMC cases have a smaller region of enhanced density and lower values than for substorm phases. The density is also depleted in the tail during SMC, similar to the substorm recovery case.

[25] Figure 7 shows contours of average ion temperature (keV) in the same manner as Figure 6. Generally, the highest temperatures are in the near-Earth region. Quiet intervals show low temperatures in the midtail, while enhanced geomagnetic activity correlates with higher temperatures in the tail (shown statistically by *Baumjohann et al.* [1989] and *Huang and Frank* [1994]). There is also evidence for dawn-dusk asymmetry, previously reported by *Wing and Newell* [1998] and *Wang et al.* [2006], with higher temperatures occurring on the duskward side of the tail. The temperature in the tail increases through the substorm phases, from growth to expansion to recovery. This agrees with *Baumjohann et al.* [1991], who used superposed epoch analysis to show that temperature increases during substorm onset and peaks during the recovery phase. Here we see a very significant difference between the Pre-SMC and SMC states versus the substorm phases. The temperature in the tail during Pre-SMC and SMC is much hotter, and the hot region is broader in azimuthal extent, compared to the temperature in all three of the substorm phases. Substorm recovery averages 7–8 keV in the mid-tail compared to >10 keV for the SMC state.

[26] Figure 8 shows contours of average total pressure (nPa) ($P_{total} = nkT + \frac{B^2}{2\mu_0}$), again in the same manner as

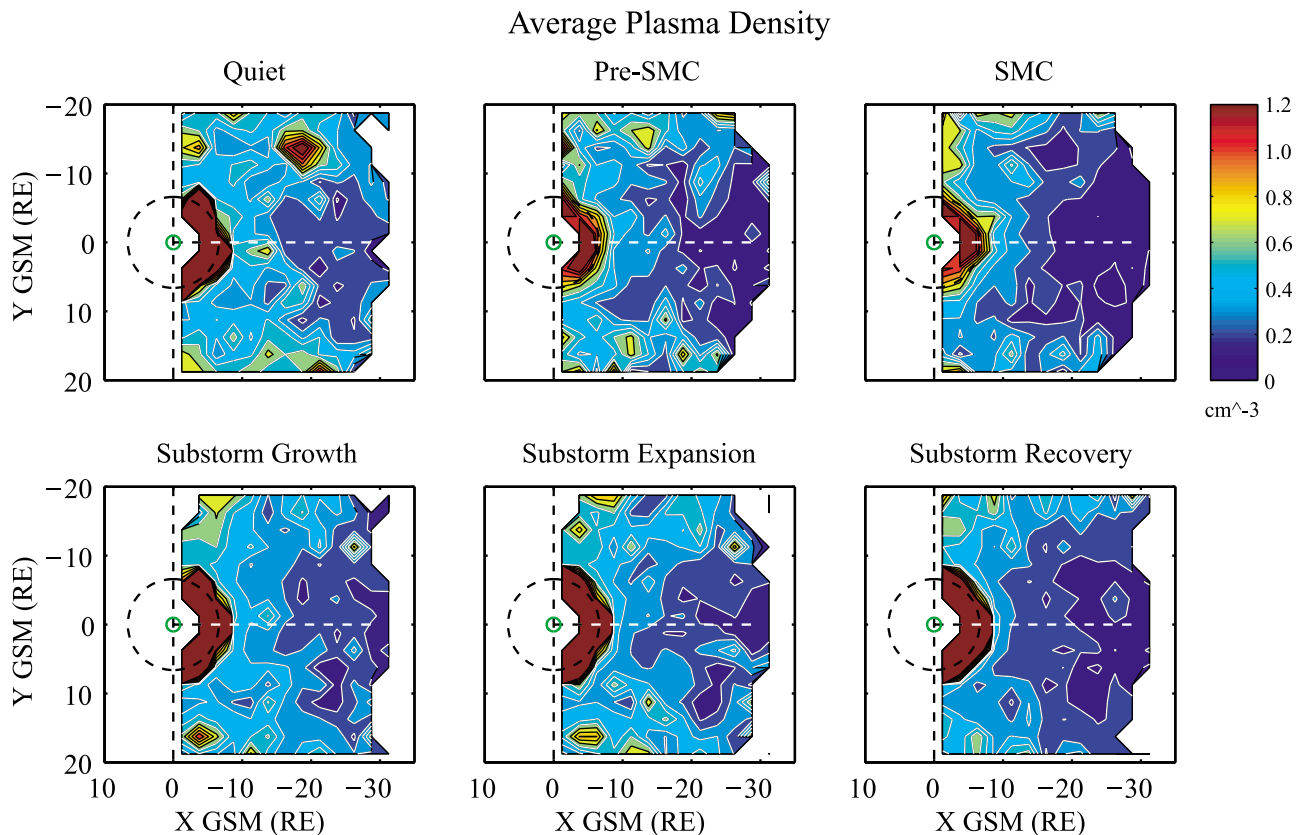


Figure 6. Contour maps of average density values in the X-Y GSM plane by type of activity: (top) quiet, pre-SMC, and SMC and (bottom) substorm growth, expansion, and recovery. All plots are to the same color scale.

Figure 6. Each case shows that pressure is higher in the inner magnetosphere and lower in the midtail. The falloff of pressure as the radial distance increases down the tail has been shown previously in numerous studies [e.g., *Spence et al.*, 1989; *Kistler et al.*, 1992; *Huang and Frank*, 1994; *Hori et al.*, 2000]. This high pressure region is largest in the SMC case, extending out radially to $\sim 12\text{--}15 R_E$. Similarly, the Pre-SMC high pressure region extends out to $10\text{--}12 R_E$. In contrast, the high pressure region during substorm recovery only extends to $\sim 8\text{--}10 R_E$. The gradient between high inner magnetosphere pressure and low midtail pressure is much steeper in the substorm growth, expansion, and recovery cases than for Pre-SMC and SMC.

[27] Figure 9 shows contours of average Earthward flux transport rate in the same format as Figure 6. The average Earthward flux transport rate was calculated by multiplying the equatorial speed, V_{x-y} , by B_z when the flow had a positive V_x . Thus, this is an average measure of how much magnetic flux is transported Earthward. During the quiet case, flux transport rates are low in the tail. The other five cases show higher rates of flux transport at various locations in the tail. During the SMC state, the highest rates of flux transport are observed on the dawn flank and throughout in the midtail. The Pre-SMC state is similar, with higher rates of flux transport on the dawn flank and in the dawnward midtail. The substorm expansion case has a region of higher flux transportation rate in the inner magnetosphere, extending radially outward along midnight. Substorm recovery also

has a region of increased flux transportation rate in the inner magnetosphere extending toward dusk, and higher flux transport rates in the midtail, similar to the SMC case.

[28] To compare the plasma conditions between types of activity in a quantitative manner, we divide the magnetosphere into two regions: tail ($\rho \geq 15 R_E$) and inner magnetosphere ($\rho < 15 R_E$). We chose this distance since it is at $15 R_E$ that fast flows during SMC experience more significant deflection (seen in Figure 5) and where the high pressure contours extend in the SMC case (Figure 8). All data within each region are then compiled into cumulative probability distribution functions (cdfs). Figure 10 shows four cdf plots for density (top left), total pressure (top right), temperature (bottom left), and Earthward magnetic flux transport rate (bottom right) within the tail region. The colored lines represent types of activity in the same way as Section 3: quiet (purple), substorm growth (green), substorm expansion (blue), substorm recovery (red), Pre-SMC (orange), and SMC (black). In all four of the plasma parameters, there is a clear separation of behavior by type of activity. SMC intervals have the lowest density, highest temperature, highest total pressure, and highest rates of Earthward flux transport out of all the modes of response.

[29] The tail region is most dense during quiet intervals. The density distributions for substorm growth and expansion are very similar, as are the Pre-SMC and substorm recovery distributions. Higher density values are more likely to be observed during substorm growth/expansion than during

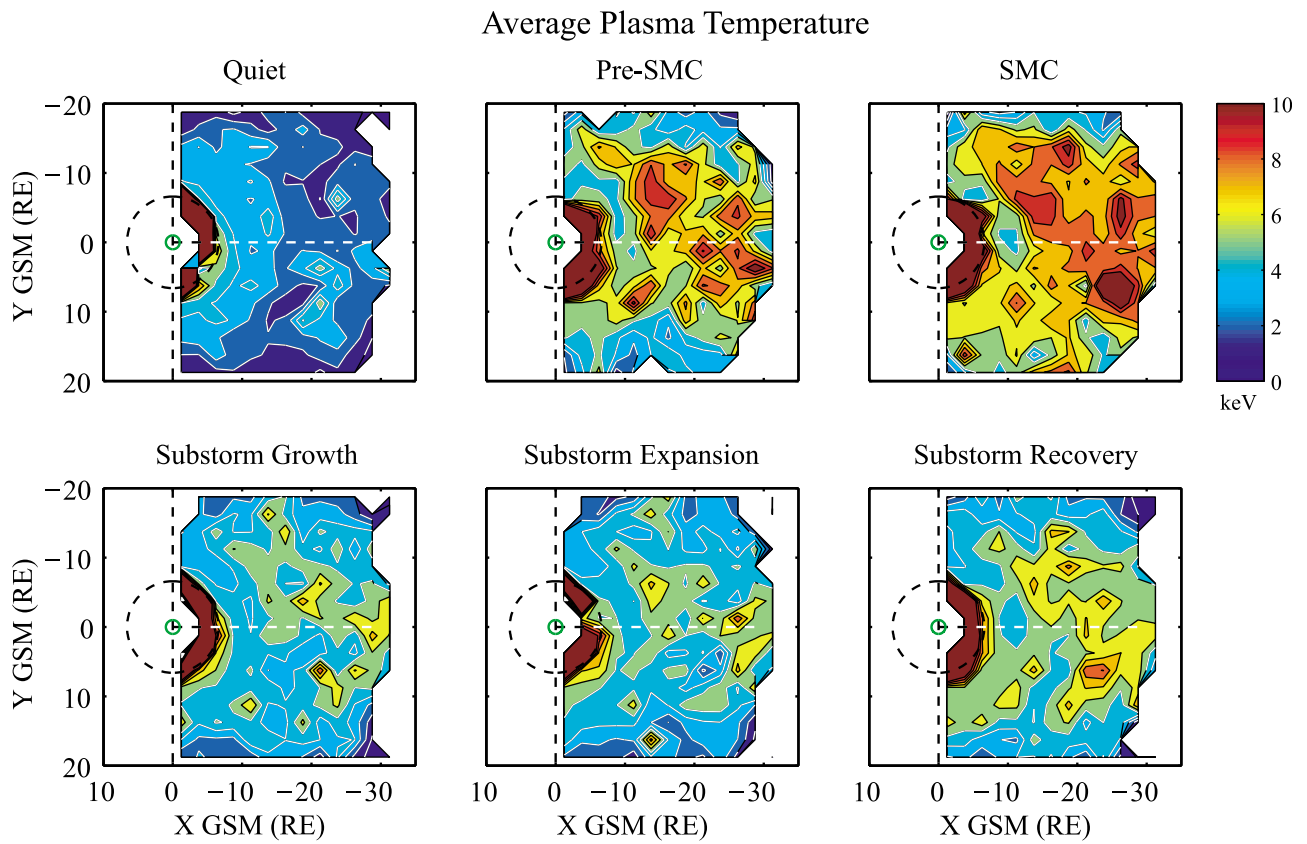


Figure 7. Contour maps of average temperature in the same format as Figure 6.

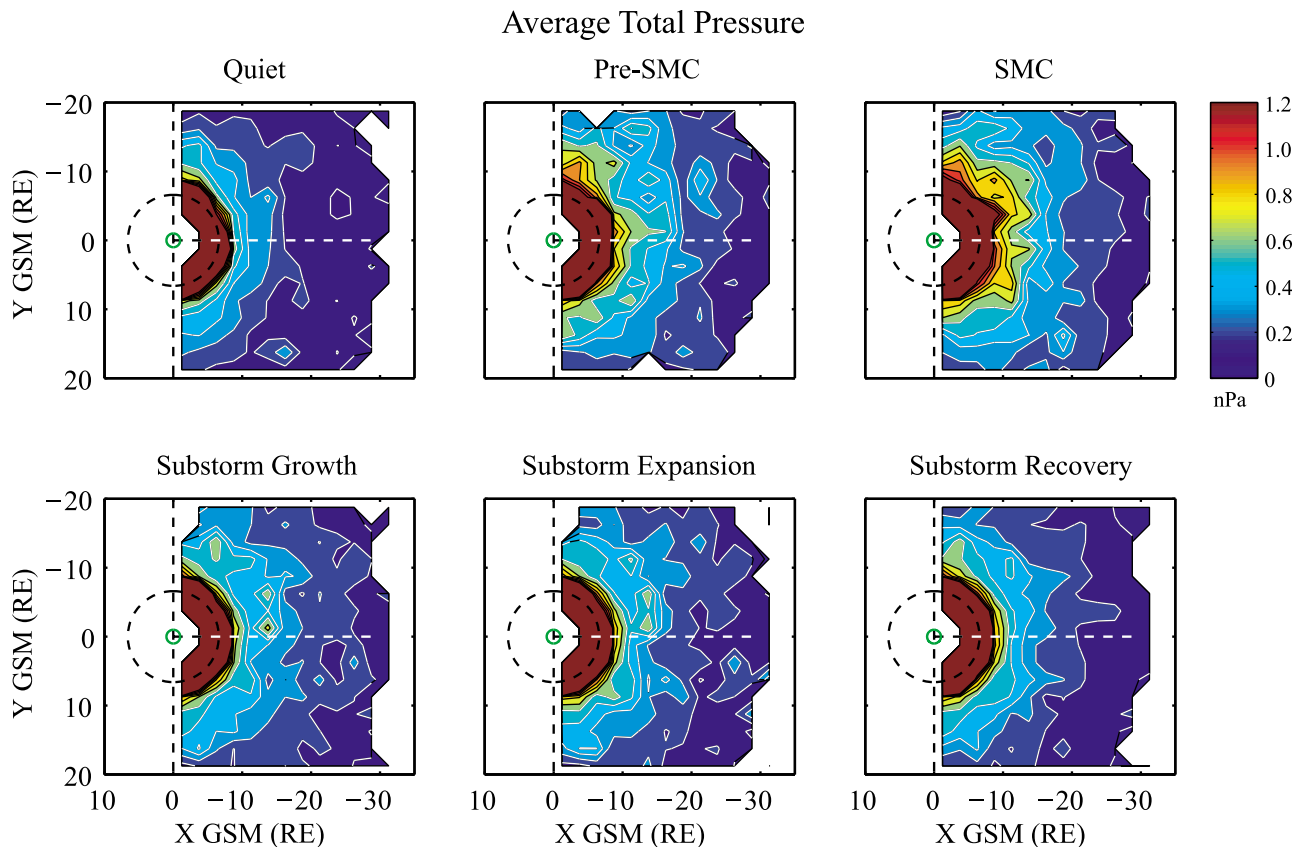


Figure 8. Contour maps of average total pressure in the same format as Figure 6.

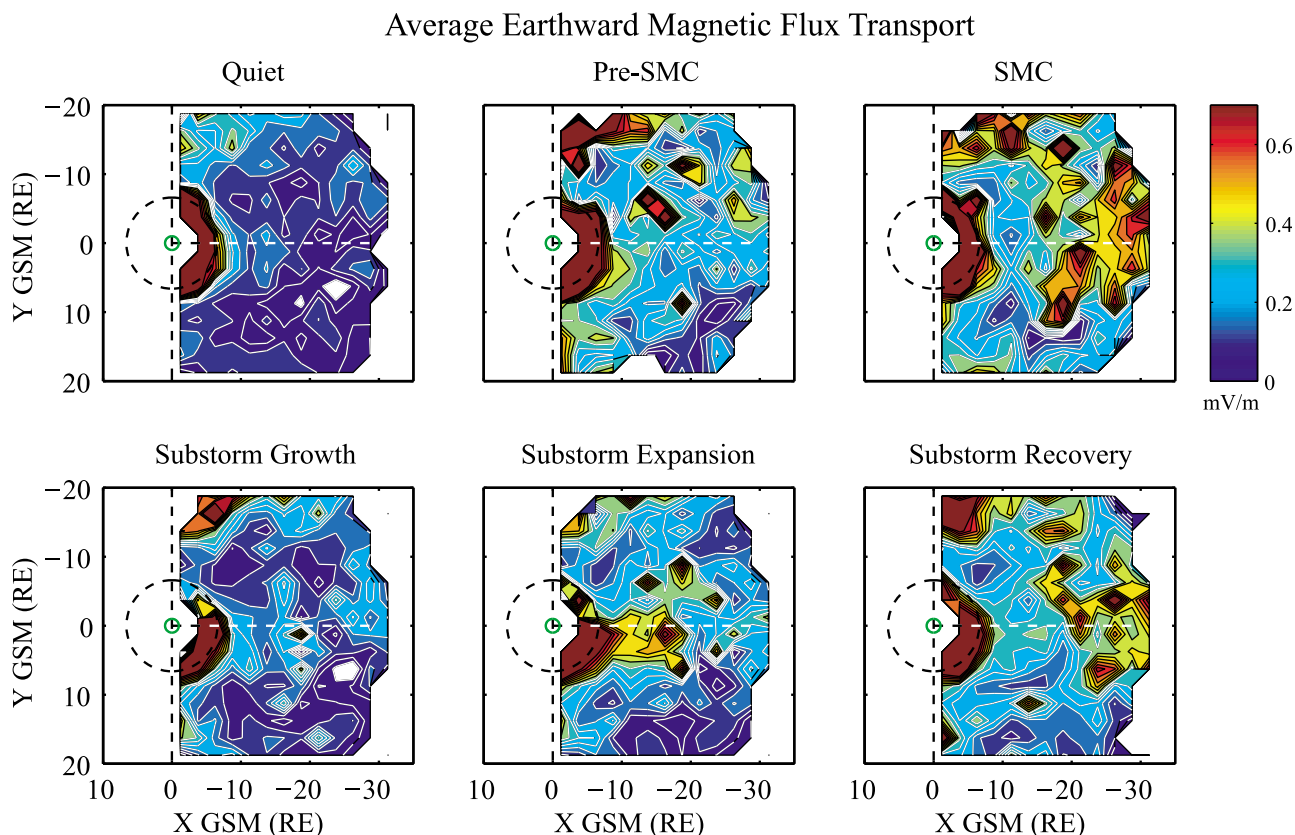


Figure 9. Contour maps of average Earthward magnetic flux transport in the same format as Figure 6.

substorm recovery/Pre-SMC. The lowest density distribution occurs during SMC. The temperature cdfs are similarly separated by the type of activity, but in reverse order: the distribution during quiet times shows the lowest temperatures, increasing through the substorm phases, with the Pre-SMC and then the SMC case showing the highest distribution of temperatures. Pre-SMC and SMC have a higher probability of higher temperatures. This concurs with the behavior in the contour plots of Figure 7, but illustrates the ordering of temperature in the tail region by type of activity. This is likely a consequence of the greater occurrence of fast flows during SMC, as the temperature increases sharply at the time of a fast flow [e.g., Angelopoulos *et al.*, 1992], in particular at times just behind dipolarization fronts observed within the fast flow interval [Runov *et al.*, 2009, 2011]. The increased occurrence of fast flows and the amount of magnetic flux they transport during SMC (Table 1) also influences the cdfs of Earthward flux transport rate, which are also very well ordered by type of activity in the same pattern as temperature. Quiet times have the lowest rates of Earthward flux transport, and the distributions increase from substorm growth/expansion, substorm recovery/Pre-SMC, and ending in the SMC distribution with the largest probability of enhanced Earthward flux transportation rate. Finally, the total pressure in the tail region increases with the mode of response, with the lowest pressure distribution during quiet intervals, higher pressure during substorm phases, and the highest pressure during Pre-SMC and SMC.

[30] Figure 11 shows cdfs of plasma conditions in the same manner as Figure 10, but in the inner magnetosphere

region ($\rho < 15 R_E$). The density in the inner magnetosphere is nearly the same for all types of activity (quiet and substorm growth distributions have been removed for clarity). The inner magnetosphere total pressure shows the same type of ordered behavior by type of activity as the tail pressure did in the previous figure. The lowest pressure distributions occur during quiet time, pressure increases through the substorm phases, and the SMC case has the highest pressure distributions. Interestingly, the Pre-SMC distribution most closely matches the substorm recovery distribution. This result matches well with the pressure contours shown in Figure 8, and shows quantitatively that the region of high pressure in the inner magnetosphere during SMCs is not just larger in extent, but also in magnitude. The temperature in the inner magnetosphere shows the same order, increasing slightly through the substorm phases from growth to recovery. Pre-SMC and SMC have the highest temperatures. Finally, the distributions of Earthward flux transport rate are similar for substorm expansion, substorm recovery, Pre-SMC, and SMC states, enhanced from quiet and substorm growth levels.

[31] To illustrate the relative changes between the tail region and the inner magnetosphere by type of activity, Figure 12 displays radial cuts along midnight of density, total pressure, temperature, and Earthward flux transport rate. Only cuts for SMC (black), Pre-SMC (orange), substorm expansion (blue), and substorm recovery (red) are shown for clarity. These figures reiterate the previous results but show where in the tail region transitions in plasma parameters occur. The ordering of density is difficult to

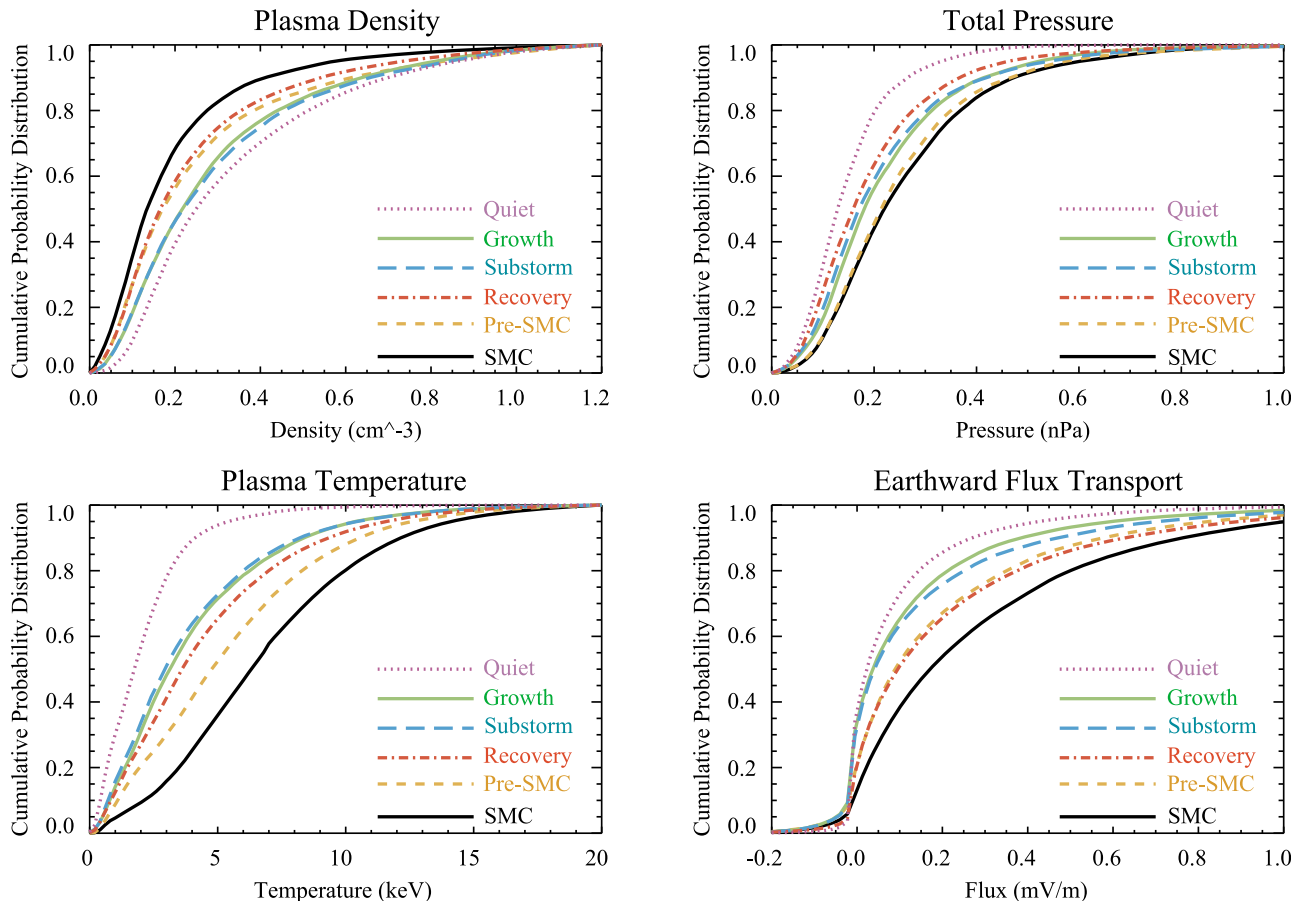
Average Tail ($\rho > 15 R_E$) Conditions

Figure 10. Cumulative probability distributions of (top left) density, (top right) total pressure, (bottom left) temperature, and (bottom right) Earthward magnetic flux transport in the tail region ($\rho > 15 R_E$). Colored lines represent each type of activity: quiet (purple dotted), substorm growth (green dotted long dashed), substorm expansion (blue long dashed), substorm recovery (red dotted short dashed), Pre-SMC (orange short dashed), and SMC (solid black).

discern in this plot, but in general the SMC case has the lowest average density values from $\sim 16 R_E$ outward. The pressure increases above substorm levels for Pre-SMC and SMC states starting as far out as $20 R_E$ and is significantly higher by $16 R_E$. The temperature in the tail region is significantly enhanced for Pre-SMC and SMC states compared to the two substorm phases. Note that the sharp drop in temperature at $12 R_E$ is not real, but is due to which satellite dominates the coverage (Geotail beyond $12 R_E$, THEMIS within $12 R_E$), and the fact that the satellites cover different time ranges (Geotail includes the rising phase and solar maximum, while THEMIS measurements occur during solar minimum).

5. Discussion

[32] This is the first statistical survey of magnetotail conditions during steady magnetospheric convection. Our goal was to investigate how the return of closed flux from the nightside to the dayside during SMC is accomplished. To do so, we identified the relative differences in the magnetotail according to the mode of magnetospheric response,

particularly focusing on SMC events and substorms. Previous case studies on SMCs have shown that during such events the magnetotail exists in a hybrid state, with a thin near-Earth current sheet (similar to the growth phase) and thick midtail plasma sheet (resembling the substorm recovery phase) [Sergeev *et al.*, 1994]. We have examined the magnetic field B_z component in the magnetotail for our events (not shown) and our statistical result agrees with these case studies. The average SMC B_z matches substorm growth phase values within $8 R_E$ and matches substorm recovery phase values outside of $13 R_E$, with a transition region between 9 and $12 R_E$.

[33] SMC events are intervals of balanced reconnection [DeJong *et al.*, 2008] in which the opened and closed magnetic flux of the magnetosphere remains stable [Milan *et al.*, 2007]. The dayside reconnection rate and the day-to-night flux transport rate are controlled by the solar wind. If the solar wind driver is enhanced and stable, the nightside x-line can match the dayside reconnection rate for hours [McPherron *et al.*, 2005]. This balance of flux reconnection rates drives convection such that flux neither accumulates in the tail nor is significantly depleted at the dayside. Closed flux must return

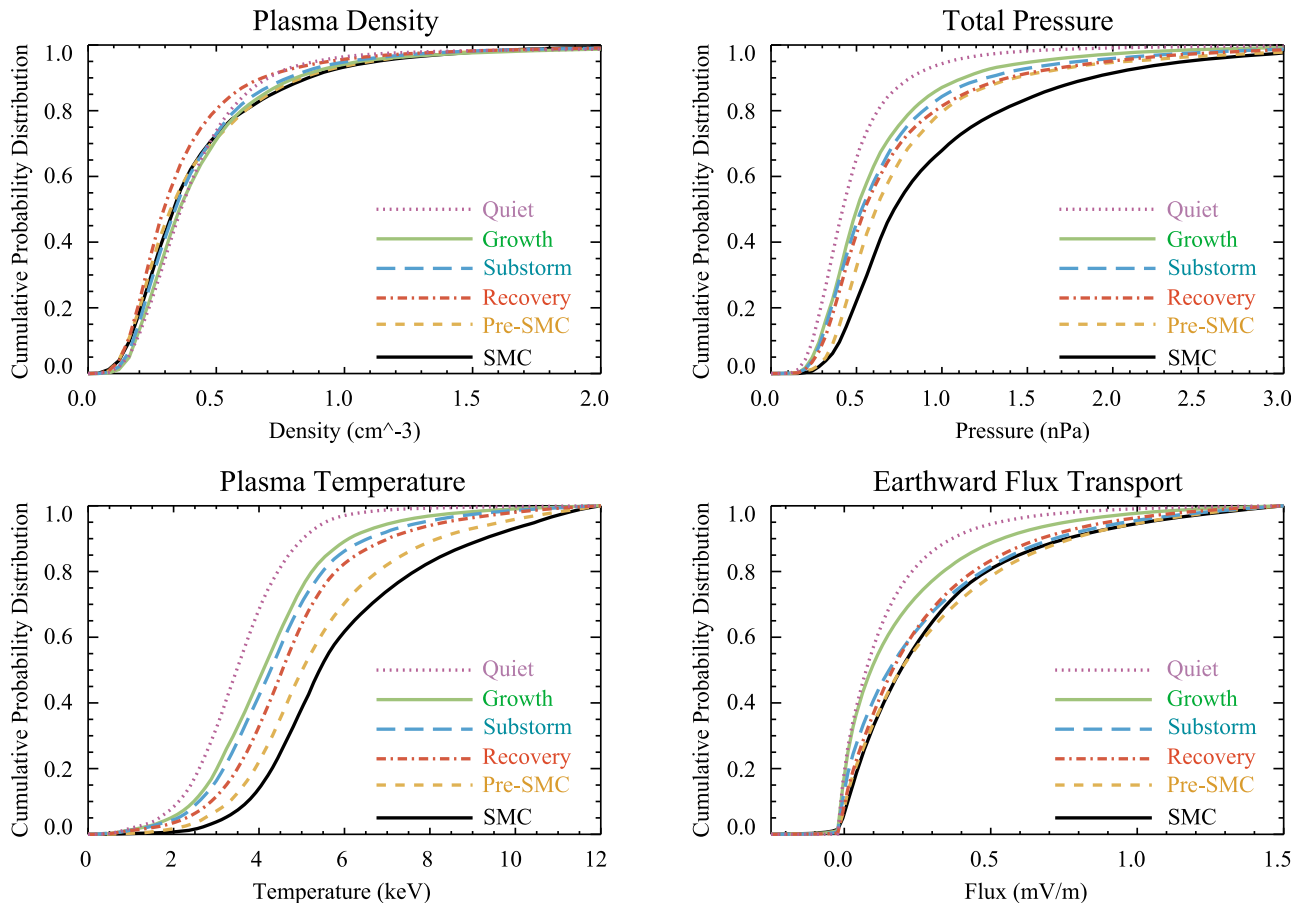
Average Inner ($\rho < 15 R_E$) Conditions

Figure 11. The same as Figure 10 except within the inner magnetosphere region ($\rho < 15 R_E$).

to the dayside in order for this to occur. More than 80% of SMC events occur within 75 min after an obvious substorm expansion [McPherron *et al.*, 2005], suggesting that such events begin with a near-Earth neutral line that moves to the midtail and remains there for the duration of the SMC, reconnecting tail lobe flux. Our results can be understood in terms of the balanced reconnection model and explain how the return of magnetic flux is accomplished.

[34] SMC events have the highest occurrence rate of fast Earthward flows ($\sim 4\%$) and these fast flows transport a larger percentage of the total magnetic flux observed ($\sim 20\%$ on average), compared to the other modes of activity (Table 1). This confirms that during SMC, magnetotail reconnection occurs throughout the event in a bursty manner. Since fast-moving plasma is responsible for a larger percentage of the total Earthward magnetic flux transport, this implies that enough flux returns to the dayside “quickly enough” to balance the rate of dayside reconnection. Additionally, the probability of observing an Earthward fast flow during SMC increases with radial distance. This suggests that the average location of the nightside x-line is in the midtail beyond $31 R_E$, in agreement with previous studies [Sergeev *et al.*, 1996].

[35] Fast flows during SMC experience a pattern of diversion toward either the dawn or dusk flank (Figure 4). This pattern is fairly symmetric around midnight, and the

deflection of flows increases as radial distance decreases. Fewer flows penetrate the inner magnetosphere (within $15 R_E$) for SMC than any other active mode of response. Those that are observed show extreme flankward deflection. This stands in marked contrast to the pattern during isolated substorms, in which closed flux from the near-Earth neutral line is injected into the nightside inner magnetosphere and forms a “pile-up region” [Baumjohann *et al.*, 1999]. Instead, fast flows carrying recently closed magnetic flux are forced away from the inner magnetosphere and the flux is returned to the dayside, likely by way of the dawn and dusk flanks. This return allows for the continued balance of reconnection rates.

[36] SMCs show higher levels of pressure than substorms, particularly in the inner magnetosphere where a broad region of enhanced total pressure extends to $>15 R_E$. This enhanced pressure region is responsible for the diversion of fast flows observed during SMC events. Consider two Earthward fast flows, one during SMC and the other during a substorm expansion. The substorm flow moves radially inward until it reaches the strongly dipolar region of the inner magnetosphere, where the total pressure increases sharply. The flow is braked in this region [Shiokawa *et al.*, 1997]. The incoming SMC flow will experience a force exerted by the pressure gradient at farther radial distances. This gradient is more gradual than the sharp gradient during substorms, and is not strong enough to stop the flow completely. Instead, it

Plasma Parameters Along Midnight Meridian

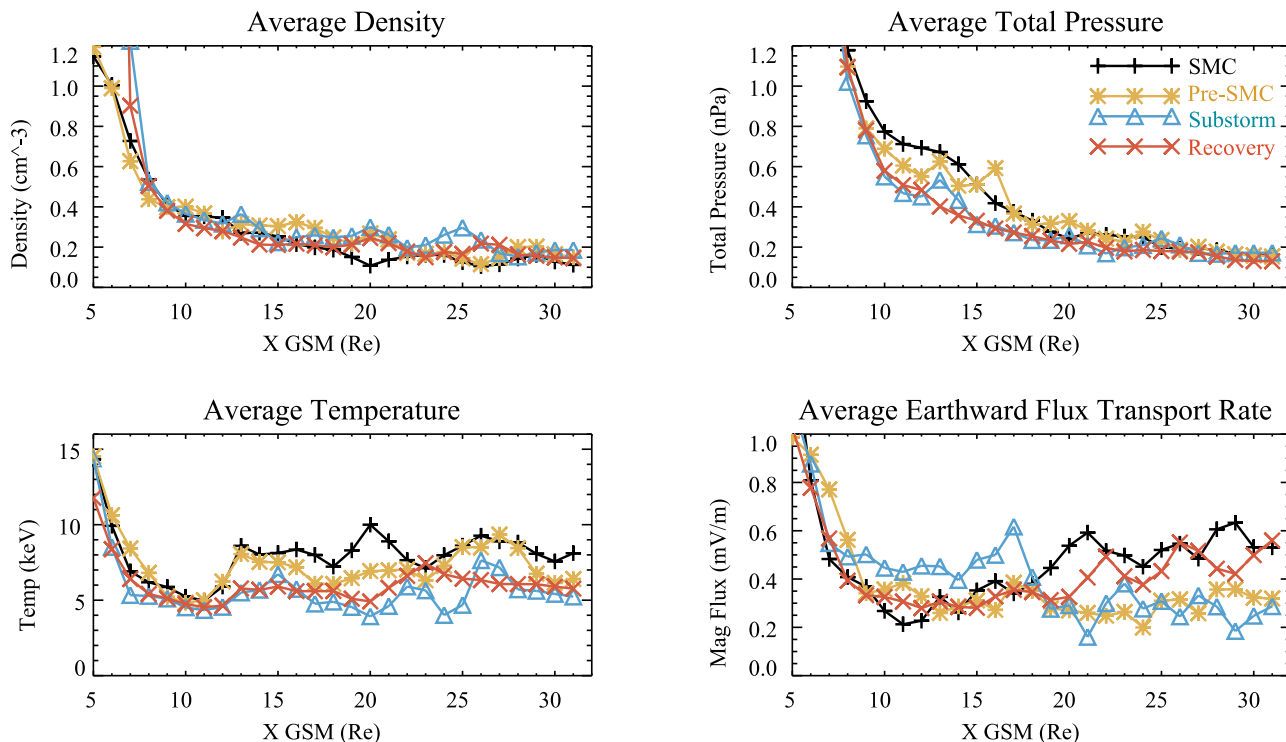


Figure 12. Average plasma parameters along the midnight meridian (within $|Y| < 5 R_E$): (top left) density, (top right) total pressure, (bottom left) temperature, and (bottom right) Earthward magnetic flux transport. Four types of activity are shown: substorm expansion (blue), substorm recovery (red), Pre-SMC (orange), and SMC (black).

deflects the flow in the direction of lower pressure (duskward if the flow is on the dusk side of midnight, dawnward if the flow is on the dawn side). The elevated inner magnetosphere pressure diverts magnetic flux to the flanks, after which flux returns to the dayside.

[37] Of the six modes of response we studied SMC events have the lowest densities and highest temperatures in the tail region. This is particularly evident for temperature, which is significantly ordered by the mode of response throughout the entire plasma sheet. The temperature is lowest and the density is highest during quiet times; temperature increases and density decreases during substorm growth/expansion and substorm recovery. The Pre-SMC temperature lies between substorm recovery and SMC levels while Pre-SMC density is similar to the substorm recovery phase. Beyond $\sim 12 R_E$, temperature during SMC events averages $\sim 7\text{--}10$ keV, well above other modes of response. In the inner magnetosphere, the temperature values remain higher than the substorm phases. The differences in density and temperature can be described in terms of the near-Earth neutral line model [McPherron *et al.*, 1973; Russell and McPherron, 1973] as follows: During the substorm growth phase, reconnection has begun in the near-Earth plasma sheet, but it occurs on closed field lines containing higher-density plasma. The substorm expansion phase begins when the x-line “eats through” the plasma sheet field lines and reaches the lower-density lobe field lines. In the recovery phase, reconnection continues on lobe field lines and the x-line retreats down the tail. Now, consider the SMC case. The interval is initiated

with a preceding substorm (Pre-SMC), but instead of the x-line retreating to the distant tail, reconnection continues in the mid-tail for hours at a time. This x-line is reconnecting lobe field lines, and so continuously sends lower-density plasma into the plasma sheet. If the nightside x-line is reconnecting lower-density lobe plasma, it must heat the plasma in order for the plasma pressure to remain the same.

[38] The rate of Earthward transportation of magnetic flux is enhanced during all active modes of response compared to quiet time. During substorm expansions, enhanced flux transport rate occurs predominantly along the tail in a region offset duskward from the midnight meridian by about $3 R_E$. During SMC and substorm recovery phases, significant Earthward flux transportation rates are seen throughout the tail region, with the highest levels occurring during SMC. In the inner magnetosphere, flux transport rate distributions are the same for substorm expansion, recovery, Pre-SMC, and SMC cases. Increased Earthward flux transport rates during SMC results in more magnetic flux to be returned to the dayside and allows for balance of the solar wind driving rate.

[39] We examined the two hours before SMCs and found that the occurrence rate of fast flows during Pre-SMC times is slightly larger than during substorm recovery, while the radial probability distribution is comparable to that during substorm expansion phases. The density, temperature, pressure, and Earthward flux transport rates in the tail region and the inner magnetosphere region for Pre-SMC lie between the SMC state and the substorm phases. In particular, the inner magnetosphere high pressure region extends farther out

during Pre-SMC, as in the SMC case, although the values are not quite as high. As most SMCs begin with a substorm, it seems that this preceding substorm expansion sets up the state of the magnetotail to assist the occurrence of SMCs.

6. Conclusion

[40] We have shown how the magnetotail accomplishes night-to-day transport of magnetic flux during balanced reconnection. During SMC events, few fast flows penetrate the inner magnetosphere; most are diverted to either flank of the magnetotail due to strong pressure gradients in the inner magnetosphere. These fast flows carry a significant portion of magnetic flux, and presumably then return to the dayside to balance the rate of reconnection at the dayside subsolar point and allow the SMC event to continue. The broad high pressure region in the inner magnetosphere is the likely result of the preceding substorm during the Pre-SMC interval, which causes the initial buildup of pressure.

[41] **Acknowledgments.** We thank the World Data Center for Geomagnetism, Kyoto, for the use of the provisional AL and AU data. Geotail magnetic field and plasma data were provided by S. Kokubun and T. Mukai via CDAWeb. We acknowledge D. Larson and R. P. Lin for use of SST data; C. W. Carlson and J. P. McFadden for use of ESA data; and K. H. Glassmeier, U. Auster, and W. Baumjohann for the use of FGM data. This paper is based upon work supported by the National Science Foundation under agreement ATM-0720422, by NASA NNX10AF25G and NASA NNX10AE61G, and by the THEMIS program, supported by NASA contract NAS5-02099.

[42] Masaki Fujimoto thanks Robert Clauer and another reviewer for their assistance in evaluating this paper.

References

- Angelopoulos, V., W. Baumjohann, C. F. Kennel, F. V. Coroniti, M. G. Kivelson, R. Pellat, R. J. Walker, H. Luhr, and G. Paschmann (1992), Bursty bulk flows in the inner central plasma sheet, *J. Geophys. Res.*, *97*(A4), 4027–4039, doi:10.1029/91JA02701.
- Angelopoulos, V., et al. (1993), Characteristics of ion flow in the quiet state of the inner plasma sheet, *Geophys. Res. Lett.*, *20*(16), 1711–1714, doi:10.1029/93GL00847.
- Angelopoulos, V., C. Kennel, F. Coroniti, R. Pellat, M. Kivelson, R. Walker, C. Russell, W. Baumjohann, W. Feldman, and J. Gosling (1994), Statistical characteristics of bursty bulk flow events, *J. Geophys. Res.*, *99*(A11), 21,257–21,280, doi:10.1029/94JA01263.
- Baker, D. N., T. I. Pulkkinen, E. W. Hones Jr., R. D. I. Belian, R. L. McPherron, and V. Angelopoulos (1994), Signatures of the substorm recovery phase at high-altitude spacecraft, *J. Geophys. Res.*, *99*(A6), 10,967–10,979, doi:10.1029/93JA02719.
- Baumjohann, W., G. Paschmann, and C. A. Cattell (1989), Average plasma properties in the central plasma sheet, *J. Geophys. Res.*, *94*(A6), 6597–6606, doi:10.1029/JA094iA06p06597.
- Baumjohann, W., G. Paschmann, and H. Luhr (1990), Characteristics of high-speed ion flows in the plasma sheet, *J. Geophys. Res.*, *95*(A4), 3801–3809, doi:10.1029/JA095iA04p03801.
- Baumjohann, W., G. Paschmann, T. Nagai, and H. Luhr (1991), Superposed epoch analysis of the substorm plasma sheet, *J. Geophys. Res.*, *96*(A7), 11,605–11,608, doi:10.1029/91JA00775.
- Baumjohann, W., M. Hesse, S. Kokubun, T. Mukai, T. Nagai, and A. A. Petrukovich (1999), Substorm dipolarization and recovery, *J. Geophys. Res.*, *104*(A11), 24,995–25,000, doi:10.1029/1999JA900282.
- DeJong, A. D., A. J. Ridley, and C. R. Clauer (2008), Balanced reconnection intervals: Four case studies, *Ann. Geophys.*, *26*, 3897–3912, doi:10.5194/angeo-26-3897-2008.
- DeJong, A. D., A. J. Ridley, X. Cai, and C. R. Clauer (2009), A statistical study of BRIs (SMCs), isolated substorms, and individual sawtooth injections, *J. Geophys. Res.*, *114*, A08215, doi:10.1029/2008JA013870.
- Dmitrieva, N. P., V. A. Sergeev, and M. A. Shukhtina (2004), Average characteristics of the midtail plasma sheet in different dynamic regimes of the magnetosphere, *Ann. Geophys.*, *22*, 2107–2113, doi:10.5194/angeo-22-2107-2004.
- Dungey, J. W. (1961), Interplanetary magnetic field and the auroral zones, *Phys. Rev. Lett.*, *6*(2), 47–48, doi:10.1103/PhysRevLett.6.47.
- Goodrich, C. C., T. I. Pulkkinen, J. G. Lyon, and V. G. Merkin (2007), Magnetospheric convection during intermediate driving: Sawtooth events and steady convection intervals as seen in Lyon-Fedder-Mobarry global MHD simulations, *J. Geophys. Res.*, *112*, A08201, doi:10.1029/2006JA012155.
- Hori, T., K. Maezawa, Y. Saito, and T. Mukai (2000), Average profile of ion flow and convection electric field in the near-Earth plasma sheet, *Geophys. Res. Lett.*, *27*(11), 1623–1626, doi:10.1029/1999GL003737.
- Huang, C. Y., and L. A. Frank (1994), A statistical survey of the central plasma sheet, *J. Geophys. Res.*, *99*(A1), 83–95, doi:10.1029/93JA01894.
- Kissinger, J., R. L. McPherron, T.-S. Hsu, and V. Angelopoulos (2011), Steady magnetospheric convection and stream interfaces: Relationship over a solar cycle, *J. Geophys. Res.*, *116*, A00119, doi:10.1029/2010JA015763.
- Kistler, L. M., E. Mobius, W. Baumjohann, G. Paschmann, and D. C. Hamilton (1992), Pressure changes in the plasma sheet during substorm injections, *J. Geophys. Res.*, *97*(A3), 2973–2983, doi:10.1029/91JA02802.
- McPherron, R. L. (1970), Growth phase of magnetospheric substorms, *J. Geophys. Res.*, *75*(28), 5592–5599, doi:10.1029/JA075i028p05592.
- McPherron, R. L., C. T. Russell, and M. Aubry (1973), Satellite studies of magnetospheric substorms on August 15, 1978: 9. Phenomenological model for substorms, *J. Geophys. Res.*, *78*(16), 3131–3149, doi:10.1029/JA078i016p03131.
- McPherron, R. L., T. P. O'Brien, and S. M. Thompson (2005), Solar wind drivers for steady magnetospheric convection, in *Multiscale Coupling of the Sun-Earth Processes*, edited by A. T. Y. Liu, Y. Kamide, and G. Consolini, pp. 113–124, Elsevier, Amsterdam, doi:10.1016/B978-044451881-1/50009-5.
- McPherron, R. L., T.-S. Hsu, J. Kissinger, X. Chu, and V. Angelopoulos (2011), Characteristics of plasma flows at the inner edge of the plasma sheet, *J. Geophys. Res.*, *116*, A00133, doi:10.1029/2010JA015923.
- Milan, S. E., G. Provan, and B. Hubert (2007), Magnetic flux transport in the Dungey cycle: A survey of dayside and nightside reconnection rates, *J. Geophys. Res.*, *112*, A01209, doi:10.1029/2006JA011642.
- Mukai, T., S. Machida, Y. Saito, M. Hirahara, T. Terasawa, N. Kaya, T. Obara, M. Ejiri, and A. Nishida (1994), The Low Energy Particle (LEP) experiment onboard the GEOTAIL satellite, *J. Geomagn. Geoelectr.*, *46*, 669–692, doi:10.5636/jgg.46.669.
- Nishida, A. (1994), The GEOTAIL mission, *Geophys. Res. Lett.*, *21*(25), 2871–2873, doi:10.1029/94GL01223.
- O'Brien, T. P., S. M. Thompson, and R. L. McPherron (2002), Steady magnetospheric convection: Statistical signatures in the solar wind and AE, *Geophys. Res. Lett.*, *29*(7), 1130, doi:10.1029/2001GL014641.
- Pytte, T., R. L. McPherron, E. W. Hones Jr., and H. I. West Jr. (1978), Multiple-satellite studies of magnetospheric substorms: Distinction between polar magnetic substorms and convection-driven negative bays, *J. Geophys. Res.*, *83*(A2), 663–679, doi:10.1029/JA083iA02p00663.
- Runov, A., V. Angelopoulos, M. I. Sitnov, V. A. Sergeev, J. Bonnell, J. P. McFadden, D. Larson, K. H. Glassmeier, and U. Auster (2009), THEMIS observations of an earthward-propagating dipolarization front, *Geophys. Res. Lett.*, *36*, L14106, doi:10.1029/2009GL038980.
- Runov, A., V. Angelopoulos, X.-Z. Zhou, X.-J. Zhang, S. Li, F. Paschke, and J. Bonnell (2011), A THEMIS multicase study of dipolarization fronts in the magnetotail plasma sheet, *J. Geophys. Res.*, *116*, A05216, doi:10.1029/2010JA016316.
- Russell, C. T., and R. L. McPherron (1973), The magnetotail and substorms, *Space Sci. Rev.*, *15*, 205, doi:10.1007/BF00169321.
- Schödel, R., W. Baumjohann, R. Nakamura, V. A. Sergeev, and T. Mukai (2001), Rapid flux transport in the central plasma sheet, *J. Geophys. Res.*, *106*(A1), 301–313, doi:10.1029/2000JA900139.
- Sergeev, V. A., and W. Lennartsson (1988), Plasma sheet at $X \sim -20 R_E$ during steady magnetospheric convection, *Planet. Space Sci.*, *36*(4), 353–370, doi:10.1016/0032-0633(88)90124-9.
- Sergeev, V. A., W. Lennartsson, R. Pellinen, M. Vallinkoski, and N. I. Fedorova (1990), Average patterns of precipitation and plasma flow in the plasma sheet flux tubes during steady magnetospheric convection, *Planet. Space Sci.*, *38*(3), 355–363, doi:10.1016/0032-0633(90)90101-U.
- Sergeev, V. A., T. I. Pulkkinen, R. J. Pellinen, and N. A. Tsyganenko (1994), Hybrid state of the tail magnetic configuration during steady convection events, *J. Geophys. Res.*, *99*(A12), 23,571–23,582, doi:10.1029/94JA01980.
- Sergeev, V. A., R. J. Pellinen, and T. I. Pulkkinen (1996), Steady magnetospheric convection: A review of recent results, *Space Sci. Rev.*, *75*, 551–604, doi:10.1007/BF00833344.
- Shiokawa, K., W. Baumjohann, and G. Haerendel (1997), Braking of high-speed flows in the near-Earth tail, *Geophys. Res. Lett.*, *24*(10), 1179–1182, doi:10.1029/97GL01062.
- Spence, H. E., M. G. Kivelson, R. J. Walker, and D. J. McComas (1989), Magnetotail plasma pressures in the midnight meridian: Observations, *J. Geophys. Res.*, *94*(A5), 5264, doi:10.1029/JA094iA05p05264.

- Tanskanen, E. I., J. A. Slavin, D. H. Fairfield, D. G. Sibeck, J. Gjerloev, T. Mukai, A. Ieda, and T. Nagai (2005), Magnetotail response to prolonged southward IMF B_z intervals: Loading, unloading, and continuous magnetospheric dissipation, *J. Geophys. Res.*, *110*, A03216, doi:10.1029/2004JA010561.
- Wang, C.-P., L. R. Lyons, J. M. Weygand, T. Nagai, and R. W. McEntire (2006), Equatorial distributions of the plasma sheet ions, their electric and magnetic drifts, and magnetic fields under different interplanetary magnetic field B_z conditions, *J. Geophys. Res.*, *111*, A04215, doi:10.1029/2005JA011545.
- Wing, S., and P. T. Newell (1998), Central plasma sheet ion properties as inferred from ionospheric observations, *J. Geophys. Res.*, *103*(A4), 6785–6800, doi:10.1029/97JA02994.
- Yang, J., F. R. Toffoletto, G. M. Erickson, and R. A. Wolf (2010), Superposed epoch study of $PV^{5/3}$ during substorms, pseudobreakups and convection bays, *Geophys. Res. Lett.*, *37*, L07102, doi:10.1029/2010GL042811.